Edwin I. Hatch Nuclear Plant-Unit 2
Proposed Exemption to 10 CFR 50.46 and
10 CFR 50 Appendix K for HNP Unit 2

Enclosure 8

GNF-0000-0101-6839NP, "GNF-Ziron Basic Characteristics and Properties,"
March 2010
(Nonproprietary)

Global Nuclear Fuel

A Joint Venture of GE,Toshiba, & Hitachi

GNF-0000-0101-6839NP
Class I
March 2010

NON–PROPRIETARY INFORMATION

GNF-Ziron Basic Characteristics and Properties

INFORMATION NOTICE

This is a non-proprietary version of the document GNF-0000-0101-6839P, which has the proprietary information removed. Portions of the document that have been removed are indicated by an open and closed bracket as shown here [[ ]].

IMPORTANT NOTICE REGARDING CONTENTS OF THIS REPORT

PLEASE READ CAREFULLY

The information contained in this document is furnished solely for the purpose(s) stated in the transmittal letter. The only undertakings of GNF-A with respect to information in this document are contained in contracts between GNF-A and participating utilities, and nothing contained in this document shall be construed as changing those contracts. The use of this information by anyone other than those participating entities and for any purposes other than those for which it is intended is not authorized; and with respect to any unauthorized use, GNF-A makes no representation or warranty, and assumes no liability as to the completeness, accuracy, or usefulness of the information contained in this document.

TABLE OF CONTENTS

Page

LIST OF TABLES

LIST OF FIGURES

REVISIONS

Number	Purpose of Revision	Reference
0	Initial issue	

GNF-Ziron Basic Characteristics and Properties

GNF has developed a zirconium alloy, designated as GNF-Ziron, which has a demonstrated capability to meet specific component application requirements within GNF fuel designs. The primary reason for developing this alloy has been the general trend of the nuclear industry towards higher exposures and the desire to decrease the impact this may have on safety compliance for GNF fuel designs. As such, the focus of this development program has been to identify an alloy capable of meeting or exceeding the thermal-mechanical performance of Zircaloy, while improving the resistance of fuel components to the effects of corrosion and hydriding.

In a separate document, the technical justification to apply GNF-Ziron in GNF fuel designs is addressed; that document provides discussions on the expected benefits, in particular, hydriding and corrosion, and on assessment of thermal-mechanical methods supporting the GNF fuel-licensing due to applying GNF-Ziron instead of Zircaloy-2 as the fuel component material. In this document, a more detailed description of the composition, processing and metallurgical characteristics of GNF-Ziron is provided in Part A. Part B of this document provides a more in-depth description of the properties, specifically, physical, thermal and mechanical properties, irradiation growth, and high temperature behavior.

A. GNF-ZIRON METALLURGICAL CHARACTERISTICS

The composition, processing and metallurgical characteristics of GNF-Ziron are described in the following sections.

A.1 GNF-ZIRON COMPOSITION

Table A-1 shows the comparison of the chemical composition of GNF-Ziron with that of the industry standard (ASTM B350) Zircaloy-2 and Zircaloy-4. GNF-Ziron is characterized by an iron specification of [[ ]], which is based on a nominal composition of [[ ]] manufacturing tolerance. GNF-Ziron thus contains a higher Fe content compared with Zircaloy-2 and Zircaloy-4. The increase is small; for example, this increase is [[ ]] compared with Zircaloy-4. Compared with GNF's specification for Zircaloy-2, in which the Fe content is typically [[ ]], the increase is [[ ]]. Alongside this small increase in Fe, the Sn, Cr and Ni composition range is relatively unchanged. The Sn content is the same as the Zircaloys. The Cr content is also essentially the same; all three alloys have nominal Cr content of about 0.1%. The Ni content is the same as Zircaloy-2 (Zircaloy-4 contains no Ni nominally). It is evident from Table A-1 that the total weight percentage of alloying elements for GNF-Ziron is comparable with that specified for the Zircaloys, especially Zircaloy-2. The compositional difference of GNF-Ziron relative to Zircaloys is small [[ ]] compared with the permitted range of total alloying elements within Zircaloy-2 or Zircaloy-4 (~0.7 wt%). The resemblance in composition forms the basis for the similarity with the Zircaloys in terms of basic properties and similar response to processing parameters in terms of the metallurgical structure, including the nature of second phase particles. These similarities and the associated effect on properties are discussed in the following sub-sections.

Table A-1 GNF alloy chemical composition for GNF-Ziron and Zircaloy

Element	Zircaloy-2 (Per ASTM B350*)	Zircaloy-4 (Per ASTM B350*)	GNF-Ziron
	wt %		
Sn	1.20-1.70	1.20-1.70	[[ ]]
Fe	0.07-0.20	0.18-0.24	[[ ]]
Cr	0.05-0.15	0.07-0.13	[[ ]]
Ni	0.03-0.08	-	[[ ]]
Fe+Cr+Ni	0.18-0.38	-	-
O	0.09-0.15	0.09-0.15	[[ ]]
Zr	Bal	Bal	Bal
Total Alloy **	1.47-2.23	1.54-2.22	[[ ]]

*Except for O **Includes O

A.2 MATERIAL PROCESSING

GNF-Ziron is intended for use as fuel assembly component material in place of Zircaloy-2. An overview of the key processing steps is given below. The same processing steps are used for the manufacture of GNF-Ziron components as used for the equivalent Zircaloy-2 component. Consistent with the minor compositional change, the response of GNF-Ziron to the processing conditions is indistinguishable from that of Zircaloy-2.

The starting materials for GNF-Ziron are sponge zirconium produced from the Kroll process, clean re-cycled GNF-Ziron or Zircaloy, and additional alloying elements necessary to achieve the desired composition. The resultant ingot is arc melted multiple times to ensure uniformity. The ingot is reduced to smaller dimensions by hot forging. The forged ingot is then cut into billets in the case of material for tubes, or slabs in the case of material intended for channels.

For tubes or cladding, the billets are typically subjected to a sequence of steps including extrusion and tube reduction to form tubeshells. The tubeshells are subjected to multiple tube reductions. The actual reduction schedule is specifically developed to meet the dimensional requirements of the final product (for example, fuel cladding or water rod). For channel materials, the slab thickness is typically reduced through a series of hot and cold rolling steps to the specified channel strip thickness.

Heat treatments are conducted at various stages of the manufacture process, for example, at the billet or slab stage and after each reduction or rolling process. The final anneal of the tubes and channel strip is a full recrystallization anneal. For cladding, tubes are straightened and polished following the final anneal. The final cladding tubes are thus supplied in the polished and recrystallized condition.

The intermediate annealing conditions are chosen to render the material generally suitable for further processing. The final anneal, in conjunction with the degree of pre-anneal cold work, has a strong influence on the final characteristics, such as grain size and texture, as discussed further in later sub-sections. The annealing sequence could potentially also affect the corrosion performance of Zircaloys and has been optimized to ensure adequate corrosion performance under the wide range of typical BWR water chemistry conditions. As a measure for added corrosion margin, GNF offers [[ ]] heat treatment for the outer surface region of the cladding. [[ ]]heat treatment is typically conducted prior to or earlier than the last reduction. This heat treatment is sometimes referred to as In-Process Heat Treat or IPHT. In [[ ]] heat treatment, the tube is heated from the outside with flowing water passing through the tube bore. The intent of [[ ]] heat treatment is to provide added margin to nodular corrosion under off-normal water chemistry conditions; under typical BWR water chemistry conditions, nodular corrosion performance is adequate [[ ]]. Previous LUA programs of GNF-Ziron cover cladding with [[ ]]heat treatment.

A.3 BASIC METALLURGICAL CHARACTERISTICS

Grain Structure and Size

GNF-Ziron, and Zircaloy-2, components used in GNF's fuel designs are in the fully recrystallized annealed condition. The recrystallized structure is ensured by the annealing that is performed after the final cold reduction or rolling. The grain structure is generally typically equiaxed, and the grain size is similar as shown by the example in Figure A-1 for GNF-Ziron and Zircaloy-2 cladding that have undergone the same process sequence. The similarity in grain structure and size between the two alloys indicates a similar response to the reduction and annealing steps and is consistent with minor difference in composition, as discussed in Section A.1.

[[

]]

Figure A-1 Examples of fully recrystallized grain structure in cladding of Ziron (left) and Zircaloy-2 (right)

Texture

As shown in Table A-1, the composition of GNF-Ziron is predominantly zirconium, as is Zircaloy-2. The crystal structure of both alloys is hexagonally close packed at temperatures below the $\alpha/\alpha+\beta$ transition temperature (~865°C, 1590°F). In polycrystalline zirconium alloys, the distribution of basal planes is generally non-uniform in space. The proportion of a particular crystal plane relative to three orthogonal reference directions is often expressed in terms of a set of Kearn's F factors. The plane of most interest is the basal plane and the three reference directions are typically the longitudinal, the transverse (or circumferential), and the radial directions for cladding; for channel strips, the third reference direction is the thickness direction of the strip. The F factors for the three reference directions are usually written as the F_l, F_t and F_r. The three F parameters in essence describe the crystallographic texture of the alloy. The texture of the alloy can affect properties; for example, the axial elongation due to irradiation growth of cladding is dependent on the F_l factor for the basal plane.

The texture of zirconium alloys is dependent on the reduction/rolling schedule and on the annealing condition. Because of the similarity in composition, the development of texture in GNF-Ziron is expected to be in essence the same as that in Zircaloy-2. Figure A-2 provides a GNF-Ziron versus Zircaloy-2

comparison of the basal plane F factors for cladding and channel materials that have been produced under the same reduction or rolling sequence and annealing conditions. The results show that there are differences in the texture of cladding compared with channel material; for example, the F_l values for cladding are [[ ]]than that for channel, and F_t values for cladding are [[ ]] than that for channel. The difference is consistent with the differences in the reduction sequence for cladding and rolling for channel material. The texture data shown in Figure A-2 shows that for a given process/anneal sequence, the texture of the two alloys are equivalent. The equivalency in texture is an indication of similar response to the reduction and annealing steps and is consistent with the minor difference in composition between the two alloys.

[[

]]

Figure A-2 Comparison of texture in GNF-Ziron and Zircaloy-2 10x10 cladding (left) and channel strip (right)

Second Phase Particles

In addition to grain structure and texture, another important attribute of zirconium alloys used in light water fuel components is the dispersion of Second Phase Particles (SPPs). The SPPs are formed because the solubility for alloying elements such as Fe, Cr and Ni are very low below the solvus temperature of approximately 850°C. The distribution of the SPPs affects primarily the corrosion characteristic of the zirconium alloy. The formation and growth of SPPs are dependent on the thermal treatment history and the SPP distribution is set by the coarsening time below the solvus temperature. Typically, the SPP distribution can be controlled separately from grain size or texture, since recrystallization and texture development can occur at significantly lower temperatures than the SPP solvus temperature.

As discussed previously, GNF offers GNF-Ziron and Zircaloy-2 cladding[[ ]] the outer surface heat treatment (IPHT) [[ ]]. The SPP sizes near the cladding outer surface are thus different with or without the surface heat treatment. A comparison of SPPs in GNF-Ziron and Zircaloy-2 [[ ]] observed in a transmission electron microscope (TEM) is given in Figure A-3. The measured SPP statistics are given in Table A-2. It should

be noted that TEM examinations and SPP measurements are conducted for the purpose of obtaining a better representative description of the cladding type and are not meant to show compliance with any SPP size requirement. The results are considered typical [[ ]]of the alloy. However, there appears to be little difference between GNF-Ziron and Zircaloy-2 for a given process. The small difference in composition, namely Fe, could result in a slight increase in the number of SPPs compared with Zircaloy-2; however, this difference would not be easily quantifiable from TEM examinations.

It should be noted that the outer surface heat treatment is designed to provide added corrosion margin as a guard against off-normal water chemistry conditions. [[ ]], GNF-Ziron cladding, like Zircaloy-2, possesses adequate performance under BWR conditions. The in-reactor corrosion behavior of GNF-Ziron is discussed in a separate document. The SPP size and distribution are not expected to affect the high temperature oxidation behavior because the SPP dissolve rapidly once the solvus temperature is exceeded.

During in-reactor operation, the neutron flux induces dissolution of the SPPs. The result is a decrease in the number density of the SPPs and the SPPs can become completely dissolved at sufficiently high fluences or irradiation times. The dissolution process in effect releases the alloying elements in the SPPs into the surrounding matrix. The SPPs formed in GNF-Ziron and Zircaloy-2 are $Zr(Fe,Cr)_2$ and $Zr_2(Fe,Ni)$. The dissolution processes for the two types of SPP are different. For the $Zr(Fe,Cr)_2$ SPPs, the dissolution rate of Fe is faster than that of Cr resulting in the SPP becoming enriched in Cr as the SPP dissolves. The Cr is eventually released from any Cr enriched SPPs or remnants. In contrast, $Zr_2(Fe,Ni)$ SPPs appear to dissolve without appreciable change in the Fe/Ni ratio. Figure A-4 shows representative data on the Fe/(Fe+Cr) and Fe/(Fe+Ni) ratios for $Zr(Fe,Cr)_2$ and $Zr_2(Fe,Ni)$, respectively, in GNF-Ziron and Zircaloy-2 as a function of irradiation time. In the unirradiated condition, Figure A-4 shows that the Fe/(Fe+Cr) and Fe/(Fe+Ni) ratios for GNF-Ziron is somewhat higher than those for Zircaloy-2. The difference is consistent with the higher Fe content in GNF-Ziron and appears to be maintained as the irradiation dissolution of the SPPs proceeded. Figure A-4 also shows that the evolution of SPP composition is similar in GNF-Ziron and Zircaloy-2. In both alloys, the Fe/(Fe+Ni) ratio in $Zr_2(Fe,Ni)$ appears to remain steady with irradiation; while the Fe/(Fe+Cr) ratio for $Zr(Fe,Cr)_2$ shows a rapid decline due to preferential Fe dissolution.

Table A-2 Comparison of outer surface SPP size in GNF-Ziron and Zircaloy-2 cladding[[ ]]

[[

]]

[[

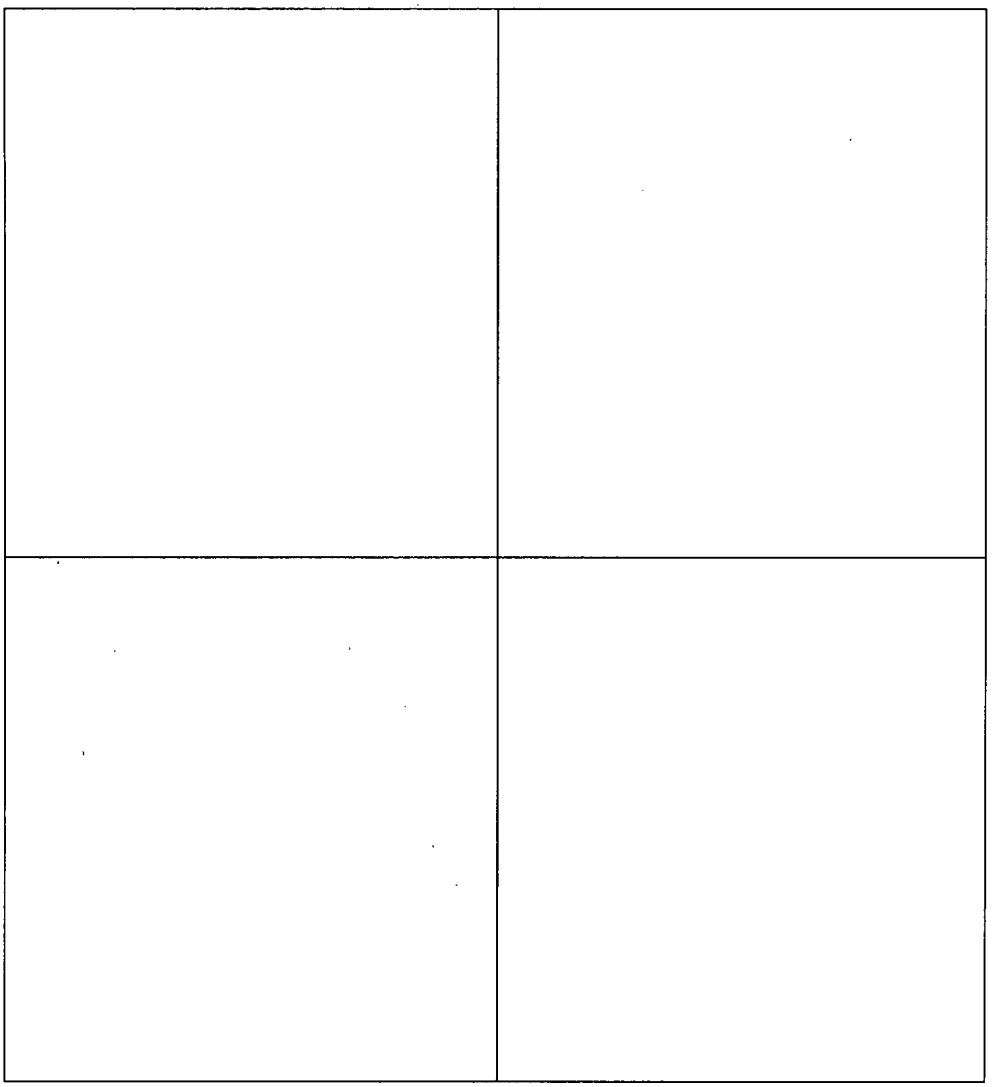

]]

Figure A-3 TEM micrograph showing SPPs in outer wall region [[ ]].

[[

]]

Figure A-4 Changes in Fe content in $Zr(Fe,Cr)_2$ and $Zr_2(Fe,Ni)$ SPPs in GNF-Ziron and Zircaloy-2.

B. MATERIAL PROPERTIES ASSESSMENT

B.1 PHYSICAL PROPERTIES

The material density and melting point are not significantly affected by the small change in Fe content between Zircaloy-2 and GNF-Ziron. The values provided in References [1] and [2] for both Zircaloy-2 and Zircaloy-4 are, therefore, applicable for GNF-Ziron and Zircaloys in general. In principle, variations are expected if chemical composition variations are significant. A single density value is typically given for Zircaloy-2 and Zircaloy-4 in References [1] and [2]. This is because the compositional differences between Zircaloy-2 and Zircaloy-4, and composition variations within the specification of each Zircaloy, are not appreciable enough to cause significant variation in the density. The alloying elements Sn, Fe, Cr and Ni can all have an effect of decreasing the melting temperature of zirconium if the compositional change is large. In contrast, oxygen has the effect of increasing the melting temperature. In Reference [2], the effect due to oxygen is specifically addressed; however, the oxygen specification for GNF-Ziron is unchanged from that of Zircaloy-2. In Reference [2], the variation in melting point due to compositional variations in Zircaloy-2 and Zircaloy-4 is typically addressed through a 20°C uncertainty. As discussed in Section A.1, the change in Fe content between GNF-Ziron and Zircaloy-2 is quite small, compared with, for example, the variation between Zircaloy-2 and Zircaloy-4. Consequently, it is appropriate to apply the Zircaloy values for density and melting point to GNF-Ziron.

B.2 THERMAL PROPERTIES

Table B-1 lists thermal properties that are insensitive to the small compositional change between GNF-Ziron and Zircaloy-2. Of these properties, specific heat, thermal conductance and thermal expansion are temperature and texture dependent; whereas emissivity is primarily sensitive to temperature and the presence of surface oxide layer. These properties are not sensitive to small changes in composition, such that Zircaloy-2 and Zircaloy-4 are generally treated without differentiation. However, specific heat, thermal conductance and thermal expansion can be composition dependent if the compositional change is large. Since the GNF-Ziron composition is a minor modification of the Zircaloy-2 composition, the thermal properties for the Zircaloys are applicable to GNF-Ziron. The thermal conductivity is discussed below as an example of equivalent thermal property despite the minor compositional difference between GNF-Ziron and Zircaloy-2.

As noted in Reference [2], the thermal conductivity is primarily a function of temperature. Other material characteristics, such as residual stress levels, crystal orientation, and minor composition differences may have a secondary influence on thermal conductivity. In this context, the compositional difference between Zircaloy-2 and Zircaloy-4 is not considered significant. In Figure B-1, the thermal conductivity of GNF-Ziron as a function of temperature is shown. The data indicate no appreciable difference between GNF-Ziron and Zircaloy-2.

The design bases for these properties are experiential correlations developed in Reference [2]. The changes in chemical composition between GNF-Ziron and Zircaloys are within the variation used to

develop this design basis. Therefore, the thermal properties of GNF-Ziron remain within the existing GNF design basis for Zircaloys.

Table B-1 Thermal Properties Unaffected by Composition Difference Between GNF-Ziron and Zircaloy

Specific Heat
Thermal Conductance
Thermal Expansion
Emissivity

[[

]]

Figure B-1 Comparison of Thermal Conductivity of GNF-Ziron with Reference Zircaloy-2 as a Function of Temperature

B.3 MECHANICAL PROPERTIES

B.3.a Modulus and Poisson's ratio

Young's modulus and shear modulus are properties that are sensitive to temperature. Young's modulus and shear modulus are also sensitive to directionality due to the presence of texture in anisotropic Zr-based alloys. Poisson ratio is generally not strongly sensitive to the temperature and texture typical of Zr-based alloys used as fuel components, and a constant value is given in Reference [2]. A differentiation of these properties based on the exact composition of the Zircaloys is generally not warranted. As the composition and texture of GNF-Ziron is similar to those of Zircaloy-2 and Zircaloy-4, Poisson's ratio, Young's modulus and shear modulus for the Zircaloys are applicable to GNF-Ziron.

B.3.b Tensile Properties

Yield and Ultimate Stress

In considering the plastic deformation behavior of Zircaloys and similar alloys, the stress-strain relationship is strongly influenced by temperature and fast neutron fluence. As temperature increases, the yield and ultimate tensile stresses generally decrease, while the ductility increases. As fast neutron fluence increases, the yield and ultimate tensile stresses generally increase, while the ductility decreases. The irradiation hardening occurs rapidly with fast neutron fluence and generally saturate at about 3.5 x 10^{25}n/m^2.

In the unirradiated condition, a number of factors potentially could affect the tensile properties. These include oxygen and tin contents and manufacture related factors such as texture and level of cold work. A range in tensile properties is, therefore, expected when measurements are taken from several production lots. The composition, other than oxygen and tin, of the Zircaloy is generally not a primary factor, such that, for example, a differentiation is not made between Zircaloy-2 and Zircaloy-4 in Reference [2]. In Figure B-2, measured tensile properties taken from GNF-Ziron cladding used in the 1999 and the more recent LUA programs are compared with a set of measurements from Zircaloy-2 cladding taken over a similar range of production period. The measurements were made in accordance with ASTM E8 "Standard Test Methods for Tension Testing of Metallic Materials" for testing at ambient temperature and ASTM E21 "Standard Test Methods for Elevated Temperature Tension Tests of Metallic Materials" for testing at elevated temperatures. As shown in Figure B-2, there is no significant difference in the yield strength, the ultimate tensile strength and the elongation between the two populations (GNF-Ziron and Zircaloy-2); however, in recognition of the variation within each population, an appreciable difference is always possible between isolated samples from the two populations. The consistency between GNF-Ziron and Zircaloy-2 in the yield and ultimate strengths shows that the strain hardening behavior of the two alloys is similar at room and elevated temperatures and that the two alloys shared similar response to temperature. The similarity in tensile properties is consistent with the minor composition difference between the two alloys and with Fe being not a strengthening alloying element in Zr.

Tensile properties of irradiated GNF-Ziron were assessed using mini-tensile specimens irradiated in the plant C and ATR reactors in the US and somewhat larger specimens irradiated in plant K reactor in Japan. The ATR irradiations were carried out at a nominal irradiation temperature of 300°C with an uncertainty of ±25°C. These specimens were discharged at fluences of [[ ]]. Companion Zircaloy-2 specimens were irradiated and discharged at fluences of [[ ]]. Following irradiation in the ATR, tensile tests were conducted at 300°C. Tests following irradiation in plant K (for up to 6 cycles of operation) were carried out at 23°C, 288°C and 343°C (300K, 561K and 616K). The highest fast neutron fluence reached was about 15 x 10^{25}n/m^2. The mechanical properties obtained from these tests are shown in Figure B-3 to Figure B-5. From Figure B-3 and Figure B-4, it can be seen that the unirradiated strength values are all higher compared with the unirradiated properties shown Figure B-2. This difference could be due to differences in detailed manufacturing methods. Also, the strengths of GNF-Ziron tested at room temperature appear to be higher compared with Zircaloy-2 in Figure B-3 and Figure B-4. This difference is likely due to the [[ ]]for the ingot used for the tested GNF-Ziron being at the upper limit of GNF's ingot chemistry specification and hence higher than that for the tested Zircaloy-2. The main purpose of Figure B-3 and Figure B-4 is to show the variation in strengths due to irradiation. The results show that GNF-Ziron behaves in the same manner as Zircaloy-2. Both alloys strengthen rapidly with irradiation and follow a similar saturating trend, and variations in the unirradiated condition remained relatively unchanged with irradiation. Overall, the limited data shown Figure B-3 and Figure B-4 appear to indicate GNF-Ziron could have slightly higher strength compared to Zircaloy-2; however, the broader set of strength data shown in Figure B-2 show that there is little difference in the strength behavior of the two alloys. For fuel component mechanical designs, the design criteria are generally based on minimum strength requirements. The strength characteristic of GNF-Ziron is bounded by Zircaloy-2.

[[

{3}]]

Figure B-2 Yield Strength (YS), Ultimate Tensile Strength (UTS) and Elongation at Room Temperature (RT) and at 343°C (ET) for GNF-Ziron and Zircaloy-2.

[[

]]

Figure B-3 Yield Strength as a Function of Fluence at room and elevated temperatures.

[[

]]

Figure B-4 Ultimate Tensile Strength as a Function of Fluence at room and elevated temperatures.

[[

]]

Figure B-5 Total Elongation as a Function of Fluence at room and elevated temperatures.

Strain

In the unirradiated condition the elongation data shown in Figure B-2 show consistent behavior between GNF-Ziron and Zircaloy-2 at room and elevated temperatures. Following irradiation, the elongation data in Figure B-5 also show consistency at room and elevated temperatures and at fluence levels up to ~10 x 10^{25} n/m^2. At the highest fluence level investigated, ~15 x 10^{25} n/m^2, GNF-Ziron showed a further reduction in elongation at elevated temperatures, while the room temperature elongation remained consistent with that at lower fluence levels. GNF-Ziron and Zircaloy-2 behaved similarly up to ~10 x 10^{25} n/m^2 with a marked difference at ~15 x 10^{25} n/m^2, where Zicaloy-2 showed significant drop in ductility at all tested temperatures. The drop in ductility of Zircaloy-2 is due to the high level of hydrogen absorption and is not an intrinsic effect of irradiation; GNF-Ziron does not show the drop to low ductility because it exhibited less hydrogen absorption. Setting aside the effect due to hydrogen absorption, the data in Figure B-5 show that GNF-Ziron and Zircaloy-2 behaved similarly with respect to irradiation effect on tensile ductility.

Degradation in tensile strain bearing capability of cladding is of interest under a number of steady state and design basis accident conditions. As shown in Figure B-5, there is little difference in the degradation of irradiation embrittlement in the absence of significant hydrogen effect. It is expected that as long as the hydrogen absorption of GNF-Ziron is less than or the same as that of Zircaloy-2, then the strain bearing behavior of GNF-Ziron under steady state or accident conditions will remain bound by Zircaloy-2 behavior.

B.3.c Perforation Stress

A correlation relating the perforation temperature for Zircaloy fuel clad under internal pressure and rapid heating conditions is currently used to assess the cladding integrity during transient events. Such a correlation is typically presented as a function of engineering hoop stress for heating rates less than 5.5°C/sec in the temperature range 650 - 1540°C. Burst tests were conducted on GNF-Ziron with target burst pressures between[[ ]]at a heating rate of [[ ]]. Figure B-6 shows the data for GNF-Ziron compared with literature data for Zircaloy obtained for a range of heating rates [3]. For clarity, only correlation lines for three heating rates are shown in Figure B-6. The comparison shows that the hoop stress for perforation of GNF-Ziron cladding falls on the same trend line as Zircaloy cladding. The perforation curve for Zircaloy-2 is therefore applicable to GNF-Ziron.

[[

]]

Figure B-6 High temperature burst test data for GNF-Ziron compared with Zircaloy correlation lines for different heating rates from [3].

B.3.d Hardness

Hardness data is used to characterize the fuel/cladding contact on the inner cladding surface of the fuel rod. Hardness is a measure of the resistance of material to plastic deformation and is dependent on tensile properties of the material as well as how the hardness test is conducted. Figure B-7 provides the performance of GNF-Ziron relative to Zircaloy-2 following irradiation in plant K and a commercial power reactor. The data suggests that GNF-Ziron may have slightly higher hardness than Zircaloy-2. However, as noted in a prior section, Figure B-3, the particular GNF-Ziron tested in plant K had somewhat stronger tensile strength characteristics than the reference Zircaloy-2. The hardness data is consistent with the strength data. In a previous section, the tensile properties of GNF-Ziron are concluded to be statistically equivalent to that of Zircaloy-2, each alloy is subject to a range of variation. Accordingly, no statistically significant difference in hardness between GNF-Ziron and Zircaloy-2 is expected based on the similarity in tensile properties.

[[

]]

Figure B-7 Hardness as a function of Fluence

B.3.e Fatigue

For the temperature range of interest to BWR applications (260 - 320°C) the cyclic stress-strain behavior of Zircaloys are related to their respective monotonic stress-strain behavior resulting from cyclic hardening and softening. Available data, Reference [2], for Zircaloys does not indicate sensitivity to the composition of Zircaloy-2 or Zircaloy-4. The data can be described using $E = bN^k$ relationship; generally two relationships are used, one for low cycle and one for high cycles to failure. Fatigue testing has been conducted on GNF-Ziron and Zircaloy-2 following up to 6 cycles of irradiation in plant K. The data are presented in Figure B-8. It is seen that GNF-Ziron and Zircaloy-2 both show similar number of cycles to failure for a given total strain amplitude. In both cases, the number of cycles to failure is consistent with reference dataset for Zircaloys, Reference [4].

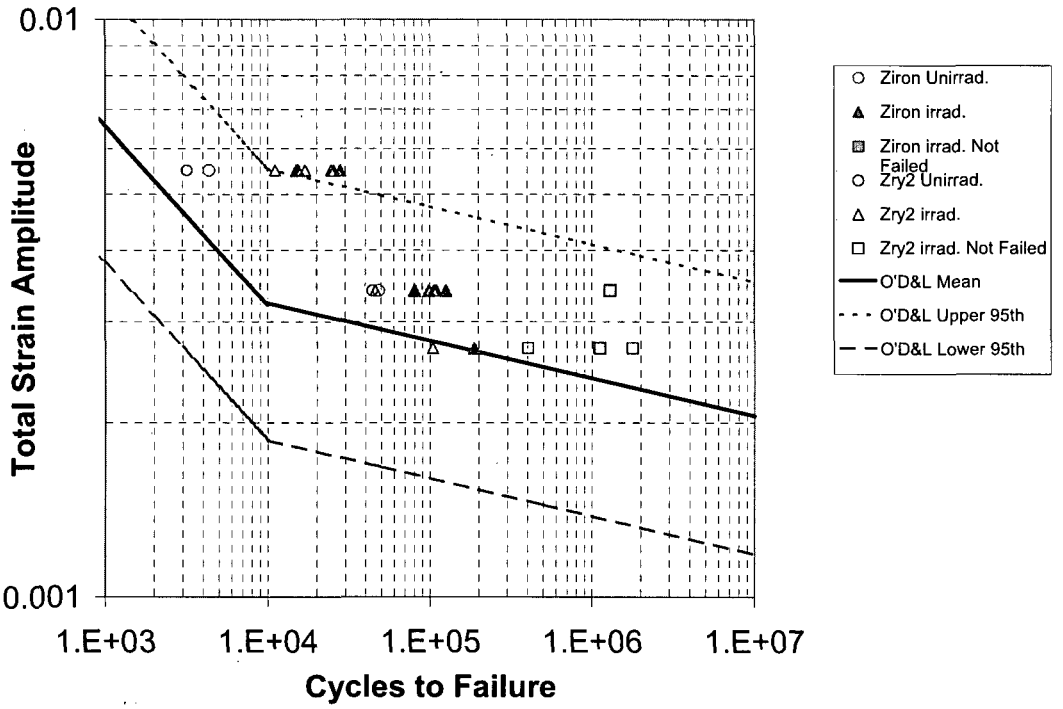

Figure B-8 Cyclic Strain Amplitude as a function of Cycles.

B.3.f Creep

Creep is dependent on the stress history of the cladding wall, including the internal gas pressure, the coolant pressure, and the fuel cladding mechanical contact forces, as well as the temperature and irradiation histories. The creep model used and approved for Zircaloy in GSTRM [5] as well as that defined for PRIME [6] is applicable to GNF-Ziron. In the irradiation program at plant K, creep specimens of GNF-Ziron, and Zircaloy-2 for comparison, pressured to 150 MPa were assessed for creep strain after 1, 2 4 and 6 cycles of irradiation at ~560K. The results are shown in Figure B-9 as a function of fast neutron fluence (E > 1MeV). The apparent results in Figure B-9 suggest creep strain for GNF-Ziron was lower than for Zircaloy-2. However, it should be noted that GNF-Ziron creep specimens accumulated less fluence than Zircaloy-2 specimen after each cycle of irradiation, i.e. the flux experienced by GNF-Ziron creep specimens (4.1 – 5.3 x 10^{17} n/m^2/s) were lower than that for Zircaloy-2 (5.6 - 7.0 x 10^{17} n/m^2/s). For Zircaloys, it is established that creep strain is dependent on fast neutron flux in the low stress regime and at the plant K irradiation temperature. The difference in measured creep strain between GNF-Ziron and Zircaloy-2 in Figure B-9 is consistent with the variation in fast neutron flux. Once flux is taken into consideration, the results in Figure B-9 suggest [[
]] between GNF-Ziron and Zircaloy-2 as shown in Figure 10.

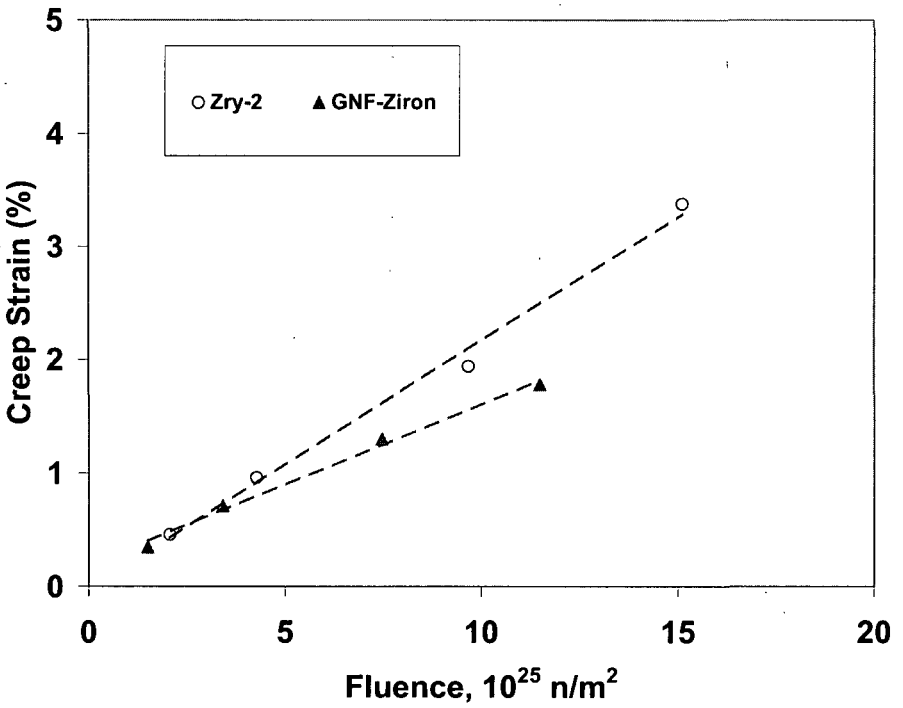

Figure B-9 Creep Strain of GNF-Ziron and Zircaloy-2 as a function of fast (E>1MeV) Fluence.

[[

]]

Figure B-10 Adjusted Creep Strain as a function of fluence for GNF-Ziron and Zircaloy-2. The strain data in Figure B-9 have been adjusted by assuming a constant flux of [[ ]].

B.4 IRRADIATION GROWTH

Previous measurements of GNF-Ziron spacer strip coupons irradiated in the ATR reactor up to a fluence level of about $6x10^{25}$ n/m^2 have shown a similar growth behavior as Zircaloy-2. In order to confirm the similarity in growth behavior at higher fluence levels, in-reactor tests were conducted in the BOR-60 test reactor. The fast neutron fluence level reached was [[ ]](E>1MeV). Because the energy spectrum in the BOR-60 reactor is different than in typical BWRs, the corresponding fast neutron fluence for BWR is numerically ~30% greater. For the irradiation growth program at BOR-60, specimens of production cladding and channel strip of GNF-Ziron and reference Zircaloy-2 were pre-characterized for texture, specifically the Kearn F-factor for basal planes. The pre-characterization of texture is important since the growth of zirconium alloys is texture dependent and is related the basal F-factor for the direction of interest through a (1-3F) term. The specimens were pre-oxidized as a measure to prevent hydrogenation of the specimens from the sodium coolant during irradiation. The growth measurements are therefore unaffected by potential contributions from hydriding. The irradiation growth results from the BOR-60 reactor are shown in Figure B-11. The data presented in Figure B-11 have been

adjusted by normalizing to a basal F-factor [[ ]] in the longitudinal direction. With this normalization, a more meaningful comparison of the irradiation growth behavior of the alloys can be made without texture effect, as indicated by the consistency between cladding and channel materials that have different measured F-factors. The results show that up to [[ ]] in equivalent BWR fluence (~11×10^{25} n/m^2 in BOR-60), GNF-Ziron and Zircaloy-2 show [[ ]]. At higher fluence levels, GNF-Ziron tended to [[ ]]. The results suggest similar irradiation growth behavior up to [[ ]]in terms of equivalent BWR fast neutron fluence or [[ ]] in terms of equivalent burnup.

Irradiation growth behavior can also be deduced from growth measurements made on fuel assembly components, such as water rods, although in these cases, other factors such as hydriding resulting from corrosion could contribute to the measured growth. In the LUA program at plant G, length measurements of GNF-Ziron and Zircaloy-2 water rods were taken at high exposures. The results are shown in Figure B-12 together with other data for Zircaloy-2 water rods at high exposures. A direct comparison is possible at [[ ]] when both GNF-Ziron and Zircaloy-2 water rods irradiated at plant G were measured. Both water rods are subject to contribution from hydriding due to corrosion. However, the average hydrogen concentrations measured in the two water rods [[ ]]. Despite the potential contribution from hydriding, the measured growth in GNF-Ziron is [[ ]] in Zircaloy-2 at high exposures and is consistent with the BOR-60 irradiation growth results shown in Figure B-11. The difference in water rod growth behavior between the two alloys [[ ]].

[[

]]

Figure B-11 Irradiation growth of cladding and strip specimens of GNF-Ziron and Zircaloy-2 irradiated in the BOR-60 reactor. The plotted data have been adjusted to a common texture [[ ]] and are shown as function of equivalent fast neutron fluence (E > 1 MeV) for the BWR at 40% void fraction.

[[ ]]

Figure B-12 Comparison of Water Rod Growth of GNF-Ziron with Zircaloy-2.

B.5 HIGH TEMPERATURE BEHAVIOR

B.5.a High Temperature Oxidation Kinetics

Oxidation kinetics under simulated LOCA conditions have been obtained for GNF-Ziron. The high temperature oxidation tests were conducted at 1000 and 1200°C (1273 and 1473K) steam. Two sets of data have been acquired for GNF-Ziron, one of which was conducted by the ANL. The resultant data are shown in Figure B-13 and Figure B-14. At 1000°C, Figure B-13, the weight gain results from both sets of tests are lower than expected based on the Cathcart-Pawel (CP) relationship. At 1200°C, Figure B-14, the weight gain results from both sets of tests are more closely matched to the expected CP relationship. Figures B-13 and B-14 show that there appears to be differences between the results obtained by the two

laboratories. One likely reason could be due to whether transient time during heat up is accounted for; the heat up transient time was accounted for by one of the two laboratories in accordance with method described in Reference [7]. The use of CP relationship for GNF-Ziron (and Zircaloy-2) is thus appropriate at 1200°C and is conservative at 1000°C.

In a recent investigation on high temperature oxidation, conducted at ANL [7], it was noted that the phenomenon of breakaway oxidation could be an additional mechanism for causing cladding embrittlement during postulated loss-of-coolant accidents conditions. The breakaway oxidation occurs when the oxidation kinetics accelerates relative to the diffusion control oxidation mechanism that is the underlying assumption for Baker-Just (BJ) and CP relationships. Breakaway oxidation can lead to a significantly increased hydrogen absorption by the cladding and result in cladding embrittlement. The net result is that the time to reach a particular Effective Cladding Reacted (ECR) could be shorter than BJ and CP predictions, and the resultant cladding embrittlement could be greater than expected based on BJ and CP relationships. The time to breakaway oxidation for a given alloy is dependent on the oxidation temperature. For most zirconium-based alloys, the shortest time before onset of breakaway oxidation occurs around 1000°C. However, the time to the onset of breakaway oxidation is alloy dependent. For the purpose of considering cladding embrittlement due to this effect, a time of greater than 5000 seconds before the onset of breakaway oxidation is considered to be very long [7]. The comparisons of oxidation kinetics GNF-Ziron at 1000°C with that predicted by the BJ and CP relationships is shown in Figure 15. From Figure B-15, it can be seen that GNF-Ziron did not exhibit breakaway oxidation at 1000°C up to 5000 seconds. The behavior of GNF-Ziron to breakaway oxidation at 1000°C is consistent with the behavior of Zircaloy-2 as reported in [7].

B.5.b Post-Quench Ductility

Two sets of data have been acquired for GNF-Ziron. The first set was obtained at ANL using the same methodology as used in Reference [7]. In the ANL work, ring compression testing was used to determine the post-test ductility at room temperature (RT) for 1000°C-oxidized rings and at 135°C for 1200°C-oxidized rings. Following oxidation at both temperatures the oxidized specimen was quenched at 800°C. The purpose for conducting these tests is to determine the level of oxidation at which the cladding becomes brittle. For ring compression tests, the criterion for embrittlement used in Reference [7] for various Zr-based alloys including Zircaloy-2 was 2% offset strain, and in Reference [8] is 1% permanent strain. The same criteria are used here for discussion on GNF-Ziron. For cladding currently used in commercial light water reactors, the embrittling oxidation level is typically greater than 15% ECR [7]. The results for offset strains versus ECR (based on CP) for GNF-Ziron together with data for Zircaloy-2 and Zircaloy-4 reported in Reference [7] are shown in Figure B-16 for 1000°C-oxidized samples and in Figure B-17 for 1200°C-oxidized samples. The results based on permanent strains are shown in Figure B-18 for 1000°C-oxidized samples and in Figure B-19 for 1200°C-oxidized samples. Two samples were tested at each oxidation level. For oxidation at 1000°C, GNF-Ziron was tested after oxidizing to four ECR levels. The results, Figures B-16 and B-18, show that GNF-Ziron exhibited ductility greater than the embrittlement criteria at room temperature for ECR (CP) [[ ]], which is the limit of testing. For oxidation at 1200°C, post-quench ductility testing was performed at three ECR levels. The results, Figures B-17 and B-19, show that both Ziron samples exhibited ductility ([[ ]]) greater than the embrittlement criteria at 135°C for 17% ECR (CP). The transition ECR (CP) for GNF-Ziron is deduced to be above but close to 17%, which was the highest ECR level

tested. Figures B-17 and B-19 shows that at 17% ECR, GNF-Ziron shows ductility similar to but slightly higher than Zircaloy-4. However, the measured offset and permanent strains for GNF-Ziron are lower than those obtained for Zircaloy-2 ([[ ]]). The ductile-to-brittle transition ECR (CP) for Zircaloy-2 was deduced to be about [[ ]] based on testing that included 20% ECR. It is possible that the transition ECR for GNF-Ziron following 1200°C oxidation could be more similar for the two alloys if additional data points had been generated for GNF-Ziron at ECR (CP) greater than [[ ]].

In addition to ring compression testing conducted at ANL, additional testing under a restraining load were conducted at ~1100°C and ~1200°C, with cladding oxidized to [[ ]] ECR (BJ) at ~1100°C and to [[ ]] ECR at ~1200°C. The results showed that cladding oxidized to [[ ]] ECR and less did not fail and that only the cladding oxidized to [[ ]] ECR failed.

[[

]]

Figure B-13 Comparison of Weight Gain for GNF-Ziron and Zircaloy-2 at 1000°C

[[

]]

Figure B-14 Comparison of Weight Gain for GNF-Ziron and Zircaloy-2 at 1200°C

[[

]]

Figure B-15 Comparison of Weight Gain for GNF-Ziron at 1000°C with Baker-Just and Cathcart-Pawel Relationships

[[

]]

Figure B-16 Post-Quench Ductility (Offset Strain) at Room Temperature for GNF-Ziron and Zircaloy-2 as a Function of ECR at 1000°C followed by quench from 800°C.

[[

]]

Figure B-17 Post-Quench Ductility (Offset Strain) at 135°C for GNF-Ziron and Zircaloy-2 as a Function of ECR at 1200°C followed by quench from 800°C.

[[

]]

Figure B-18 Post-Quench Ductility (Permanent Strain) at Room Temperature for GNF-Ziron and Zircaloy-2 as a Function of ECR at 1000°C followed by quench from 800°C.

[[

]]

Figure B-19 Post-Quench Ductility (Permanent Strain) at 135°C for GNF-Ziron and Zircaloy-2 as a Function of ECR at 1200°C followed by quench from 800°C.

C. REFERENCES

[1] Lustman, B and Kerze, F jr., The Metallurgy of Zirconium, McGraw-Hill, 1955

[2] SCDAP/RELAP5/MOD3.1 Code Manual Volume IV: MATPRO -- A Library of Materials Properties for Light-Water-Reactor Accident Analysis, NUREG/CR-6150, EGG-2720 Volume IV, 1993

[3] NUREG-0630, "Cladding Swelling and Rupture Models for LOCA Analysis"

[4] W. J. O'Donnell, B. F. Langer, "Fatigue Design Basis for Zircaloy Components", Nucl. Sci. Eng., 20, 1, (1964).

[5] Acceptance for Referencing of Licensing Topical Report NEDE-24011-P-A Amendment 7 to Revision 6, GE Standard Application for Reactor Fuel Letter, C.O. Thomas (NRC) to J. S. Charnley (GE), MFN-036-85, March 1, 1985.

[6] The PRIME Model for Analysis of Fuel Rod Thermal – Mechanical Performance, NEDC-33256P.

[7] NUREG/CR-6967, ANL-07/04, "Cladding Embrittlement During Postulated Loss-of-Coolant Accidents"

[8] Advance Notice of Proposed Rulemaking, 10 CFR Part 50 Performance-Based Emergency Core Cooling System Acceptance Criteria, Federal Register Vol. 74, No. 155, 2009.